Separation and Purification Technology 362 (2025) 131712

Contents lists available at ScienceDirect

Separation and Purification Technology

journal homepage: www.elsevier.com/locate/seppur

Synergistic inhibition of degradation and corrosion in monoethanolamine solvent for CO_2 capture solvents: Experimental and simulation studies

Yuwei Wang [a], Mengxiang Fang [a,*], Jiabao Yi [b,*], Hai Yu [c,*], Qi Yang [d], Xiaozheng Lu [a], Tao Wang [a]

[a] State Key Laboratory of Clean Energy Utilization, Zhejiang University, Hangzhou 310027, China
[b] Global Innovative Center of Advanced Nanomaterials, School of Engineering, University of Newcastle, Callaghan, NSW 2308, Australia
[c] CSIRO Energy, 10 Murray Dwyer Circuit, Mayfield West, NSW 2304, Australia
[d] CSIRO Manufacturing, Research Way, Clayton, Victoria 3168, Australia

ARTICLE INFO

Editor: Dr. S Yi

Keywords:
Amine-based solvent
Degradation
Corrosion
Carbon capture
Inhibitor
Synergistic inhibition

ABSTRACT

This study investigated the synergistic effects of six inhibitors on the degradation and corrosion of monoethanolamine (MEA) solvent used in CO_2 capture processes. A combination of experimental tests and computational simulations was employed to identify optimal inhibitor formulations that minimize both degradation and corrosion. Results demonstrated that the combination of potassium sodium tartrate (PST) and L-methionine (L-MET) significantly reduced the degradation and corrosion rates, with a 62.7 % reduction in oxidative degradation and a 98.8 % inhibition efficiency against corrosion at an optimal 1:2 ratio. Quantum chemical calculations and molecular dynamics (MD) simulations elucidated the synergistic inhibition mechanism, revealing that the corrosion inhibition effectiveness is closely associated with their electronic properties and adsorption behavior on the Fe (110) surface. The findings suggest that the PST and L-MET ratio optimization can enhance solvent performance, potentially reducing operational costs and environmental impacts associated with solvent replacement and equipment maintenance in industrial CO_2 capture applications.

1. Introduction

Chemical absorption using amine-based solvents remains one of the most mature and widely technologies implemented for post-combustion carbon capture (PCCC). Numerous long-term operational carbon capture installations worldwide attest to its commercial viability. These include, the first commercial carbon capture plant at a power station, Boundary Dam, which began operation in 2014 and captures up to 1 million tons of CO2 per year, the pilot plant at Niederaussem lignite-fired Power Station (over 28,000 h of operation), the demonstration project with an annual capacity of 150,000 tons at Jinjie Power Plant (over 10,000 h), the large-scale 500,000 tons CO_2/year industrial plant at Taizhou Power Plant (over 5,000 h), the 1 ton CO_2/hour absorption pilot at Esbjerg power plant in Denmark (over 4,000 h), and the TCM DA Amine Plant located in Mongstad (over 2,000 h) [1,2]. However, one of the most significant challenges faced by amine-based solvents during long-term operation is the degradation of the solvent, which often leads to severe equipment corrosion. These issues not only compromise the efficiency of the system but also frequently necessitate system shutdowns for maintenance [3,4]. In particular, the replacement cost of degraded solvents in the systems is estimated to account for 4–10 % of the total operational cost [5,6].

The degradation mechanisms of amines are primarily categorized into oxidative and thermal degradation [7–9]. Oxidative degradation is triggered by the presence of oxygen (O_2) in the flue gas, predominantly occurring in the absorber, while thermal degradation typically takes place in the stripper and reboiler at temperatures ranging from 100 to 125 °C, where carbamate polymerization reactions are prevalent. Notably, anaerobic cleavage of amine bonds-a form of thermal degradation-is less likely to occur under conditions of low regeneration temperatures (below 110 °C) or high O_2 concentrations in the flue gas (above 1 vol%) [10–13]. The oxidative degradation mechanism involves the catalytic reaction of dissolved metal ions with O_2, forming free radicals. These radicals further react with amines, primarily through

Abbreviations: **MEA**, Monoethanolamine; **PST**, Potassium Sodium Tartrate; **L-ARG**, L-Arginine; **L-MET**, L-Methionine; **L-CYS**, L-Cysteine; **HSS**, Heat-Stable Salts; **DFT**, Density Functional Theory; **MD**, Molecular Dynamics; **SEM**, Scanning Electron Microscopy; **XRD**, X-Ray Diffraction.

* Corresponding authors.
E-mail addresses: mxfang@zju.edu.cn (M. Fang), Jiabao.Yi@newcastle.edu.au (J. Yi), hai.yu@csiro.au (H. Yu).

https://doi.org/10.1016/j.seppur.2025.131712
Received 3 December 2024; Received in revised form 10 January 2025; Accepted 18 January 2025
Available online 20 January 2025

electron or hydrogen abstraction mechanisms [12,14–16].

The addition of inhibitors to the solvent has been explored as a viable solution to mitigate both degradation and corrosion. Inhibitors function through various mechanisms, with degradation inhibitors typically categorized as radical scavengers, oxygen scavengers, and metal chelating agents [17,18]. Among the numerous inhibitors tested, ethylene diamine tetra acetic acid (EDTA) has been identified as an effective chelating agent, although its instability in solution limits its practical application [19,20]. Supap et al. conducted studies on the effectiveness of different degradation inhibitors under varying CO_2 loadings and O_2 concentrations, ultimately identifying the mixture of $NaSO_3$ and PST (0.05 M: 0.015 M) to be particularly effective, achieving a degradation inhibition rate of 98 % [21,22]. Voice et al. studied over 100 potential degradation inhibitors and found that chelating agents were the most effective in inhibiting MEA oxidation at non-elevated temperatures. They developed a highly efficient free-radical scavenger, Inh A, which reacts with metals in the solution, rendering them insoluble or causing them to precipitate [15].

In terms of corrosion, while MEA itself is non-corrosive, its aqueous solution, particularly when loaded with CO_2, exhibits high corrosivity toward carbon steel and can even corrode stainless steel with chromium content as high as 20 wt% [23–31]. Degradation products such as heat-stable salts (HSSs) significantly accelerate the corrosion process [32,33].

Corrosion inhibitors are categorized based on their mechanisms into anodic inhibitors, cathodic inhibitors, and metal complexing agents [34,35]. Numerous inhibitors have been developed and commercialized, with inorganic inhibitors such as arsenic, vanadium, copper, cobalt, molybdenum, and antimony salts demonstrating superior performance over organic compounds in experimental settings. For example, sodium metavanadate ($NaVO_3$) has shown excellent corrosion inhibition in 2-amino-2-methyl-1-propanol (AMP) solutions, providing over 90 % protection even at the low concentration of 10 ppm [36]. However, vanadium ions may catalyze oxidative degradation in MEA-H_2O-CO_2-O_2 system [37,38].

Recent attention has focused on organic inhibitors like amino acids due to their environmentally friendly, non-toxic, and biodegradable properties. L-MET, for example, has demonstrated significant effectiveness in reducing the corrosion rate of 1018 carbon steel in MEA solution, with inhibition efficiencies of 83.6 % and 75.0 % under static and dynamic conditions, respectively [39]. L-Arginine (L-ARG) has also been found to reduce corrosion current density in MDEA solvents, achieving an inhibition efficiency of 51.54 % at a concentration of 0.1 mol/L [40]. Meanwhile, L-cysteine (L-CYS) and L-MET have shown excellent corrosion inhibition of copper in 1 M HNO_3, with inhibition efficiencies of 95.4 % and 97.3, respectively, due to the nucleophilicity of sulfur in their structures [41]. Despite advancements in individual degradation or corrosion inhibitors, few studies have focused on combined inhibition strategies [42,43]. Fytianos et al. evaluated the inhibitory effects of six compounds on both degradation and corrosion. They found that while 1,3-Diaminopropane-N, N, N', N'-tetra acetic acid (PDTA) exhibited strong degradation inhibition, its corrosion inhibition was inadequate, whereas carbohydrazide showed excellent corrosion inhibition but insufficient degradation resistance [44].

Furthermore, computational approaches like density functional theory (DFT) and molecular dynamics (MD) simulations offer atomic-scale insights into the adsorption, interaction energies, and synergistic effects of corrosion inhibitors on metal surfaces. Zhu et al. employed MD analysis to reveal that the synergistic corrosion inhibition effect of oleic acid imidazoline and L-cysteine on carbon steel, with a 3:1 ratio achieving a 95.08 % inhibition rate, was attributed to reduced adsorption energy and the formation of a bilayer adsorption film [45]. Similarly, Zhang et al. investigated the interaction between calcium lignosulfonate and inorganic inhibitors on Q235 carbon steel in an alkaline Cl^- environment, showcasing the role of synergistic interactions in enhancing corrosion resistance. Lgaz et al. discovered that the integration of amino acids enhances the bonding of triazine-based inhibitors with iron surfaces by enabling strong covalent interactions, thereby facilitating the formation of stable adsorption films for improved corrosion protection [46]. However, there is a significant gap in computational studies focusing on the inhibitors for amine-based solvent, which remains largely unexplored in the literature [47].

Building on operational insights from our 200 Nm^3/h carbon capture plant, where amino acids and salts effectively reduced degradation and corrosion, this study investigated their synergistic effects within MEA-CO_2-H_2O systems. The selection of six inhibitors shown in Table 1 was informed by prior evidence of their efficacy in mitigating degradation or corrosion, their potential for synergistic interactions, and particularly the environmentally friendly characteristics of the three amino acids, which are biodegradable and non-toxic [48]. Additionally, salts such as PST, Na_2MoO_4, and $NaVO_3$ were chosen for their industrial viability, characterized by high stability and cost-effectiveness [49,50]. Preliminary screening further demonstrated their robust individual inhibition performance, justifying their inclusion for detailed evaluation of combined effects.

Through a combination of oxidative degradation experiments, high-temperature corrosion tests, and advanced analytical techniques as well as quantum chemical calculations and molecular dynamics (MD) simulations using Materials Studio, this research aims to develop an effective composite inhibitor and elucidate its underlying inhibition mechanisms.

2. Experimental Section

The detailed information of chemicals and materials are presented in Supplementary Material.

2.1. CO_2 absorption bubbling procedure

Fig. 1 illustrates the CO_2 absorption experimental setup. The setup utilized a bubbling absorption method to prepare a CO_2 saturated absorbent solution. The detailed procedure can be found in the Supplementary Material.

2.2. Oxidative degradation experiment

The equipment used for the oxidative degradation experiment is a custom-designed and constructed forced oxidative degradation reactor, as illustrated in Fig. 2. The sealed reactor consists of a 500 mL stainless-steel reservoir, an electric heating sleeve, a magnetic stirrer, a gas inlet, a gas outlet, and a liquid sampling port. The reactor is rated for a safe pressure of 2 MPa.

The detailed experimental procedure can be found in the Supplementary Material.

Degradation degree, D (%) also referred to as the amine loss rate, represents the percentage reduction in organic amine concentration in the absorbent after degradation relative to its initial amine concentration. The calculation formula is shown in Eq. (1).

$$D(\%) = \frac{C_0 - C_t}{C_0} \times 100 \quad (1)$$

herein, C_0 is the initial amine concentration in the absorbent in mol/L, and C_t is the amine concentration in the absorbent after degradation in mol/L.

Degradation inhibition efficiency, IE_D (%) is defined by Equation (2).

$$IE_D(\%) = \frac{D_{uninhibited} - D_{inhibited}}{D_{uninhibited}} \times 100 \quad (2)$$

herein, $D_{uninhibited}$ and $D_{inhibited}$ represent the degradation degrees of the absorbent without and with the addition of inhibitor, respectively, over the same degradation time.

Table 1
Name, CAS and structure of inhibitors used in this study.

Type	Abbreviation	Compound	CAS	Chemical structure
Amino acids	L-ARG	L-arginine	74-79-3	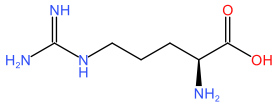
	L-MET	L-methionine	63-68-3	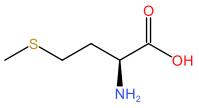
	L-CYS	L-cysteine	52-90-4	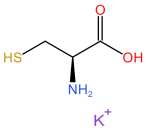
Salts	PST	Potassium sodium tartrate	304-59-6	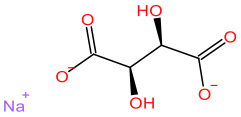
	Na_2MoO_4	Sodium molybdate	7631-95-0	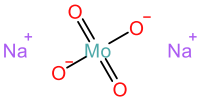
	$NaVO_3$	Sodium metavanadate	13718-26-8	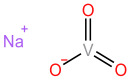

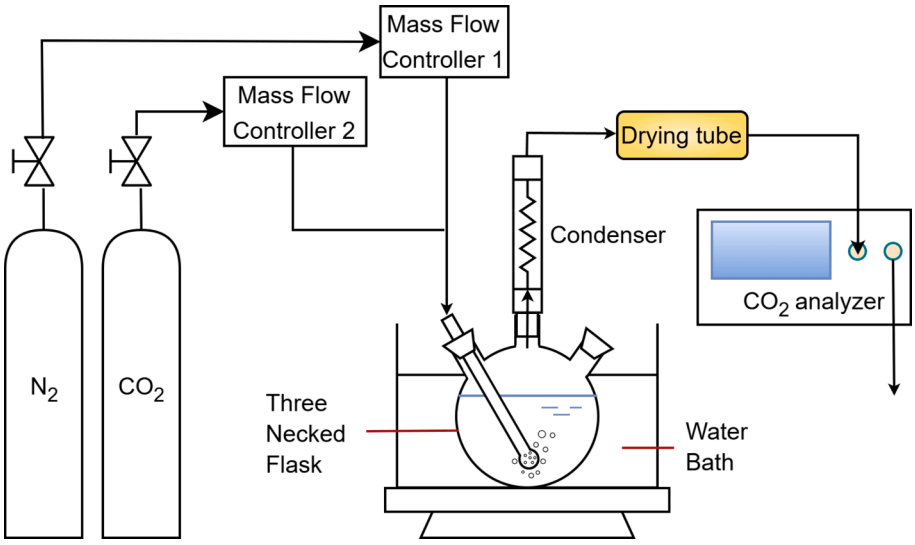

Fig. 1. CO_2 Absorption Bubbling Experimental Setup.

2.3. Immersion corrosion experiment

Q235 carbon steel, sourced from Shenzhen Quanfu Metal Co., Ltd., and conforming to the Chinese GB/T 699–2015 standard, was utilized in this study. The specific composition of the material is detailed in Table 2. Test samples with a size of 10 mm × 2 mm × 20 mm, were prepared by polishing with 240-grit and 500-grit SiC sandpaper to achieve a bright, protective film-free surface. Subsequently, the samples were ultrasonically cleaned in methanol to ensure a smooth and flat surface.

Immersion corrosion experiments were conducted using a high-temperature and high-pressure autoclave, as shown in Fig. 3. The polished carbon steel samples were placed in the Teflon liner, which was then filled with 20 ml of saturated CO_2-loaded amine solution, ensuring complete submersion of the samples. The autoclave was heated to 100 °C in an oven to carry out the experiment. After 14 days, the autoclave was removed from the oven and allowed to cool to room temperature, after which both the carbon steel sample and the solution were collected for subsequent analysis. To ensure reproducibility, all immersion experiments were repeated three times under identical conditions.

According to ASTM G1 standards, the cleaning solution for preparing metal surfaces for corrosion testing was prepared by mixing 265 ml of HCl, 1.75 g of hexamethylenetetramine, and deionized water to a total volume of 500 ml. The corroded samples were immersed in this solution

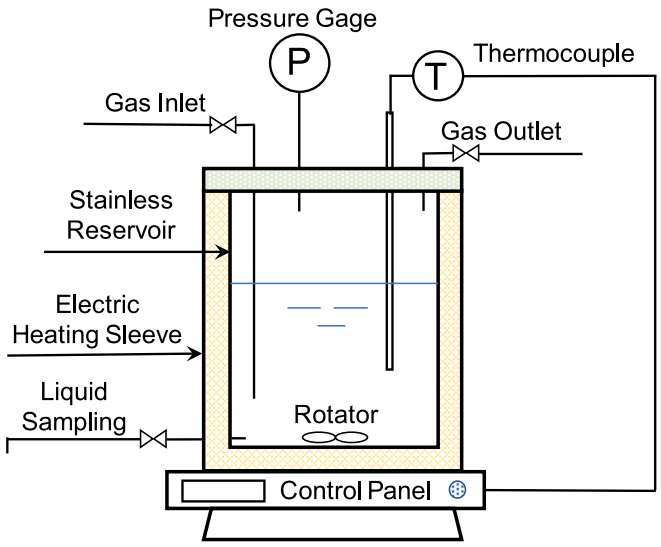

Fig. 2. Forced oxidative degradation reactor.

for 30 min to remove surface corrosion products, including protective films. After immersion, the carbon steel samples were rinsed with deionized water and methanol, dried, and quickly weighed. Corrosion rate, R (millimeters per year, mmpy) was calculated using Eq. (3).

$$R(mmpy) = \frac{87600 \times (m_0 - m_1)}{S \times \rho \times t} \tag{3}$$

herein, m_0 and m_1 are the initial weight of the sample before corrosion and the weight of the corroded sample after washing, in g. S is the surface area of the carbon steel sample, in cm^2. t is the duration of the corrosion experiment, in hours (h). ρ is the density of the carbon steel sample, in g/cm^3.

Corrosion inhibition efficiency, IE_c (%) is defined by Eq. (4).

$$IE_C(\%) = \frac{R_{uninhibited} - R_{inhibited}}{R_{uninhibited}} \times 100 \tag{4}$$

herein, $R_{uninhibited}$ and $R_{inhibited}$ represent the corrosion rates of the carbon steel samples without and with the addition of inhibitor, respectively, over the same corrosion time.

2.4. Analytical methods

Table 3 provides a summary of the methods used. Detailed information regarding the instruments, operational procedures, and experimental settings for each method can be found in the Supplementary Material.

2.5. Theoretical calculations

All inhibitor molecules were fully geometrically optimized using the DMol3 module within the Materials Studio 2020 software. Energy optimization was performed based on the Generalized Gradient Approximation (GGA) and Perdew-Burke-Ernzerhof (PBE) methods. Quantum chemical parameters, including the highest occupied molecular orbital energy (E_{HOMO}, eV) and the lowest unoccupied molecular orbital energy (E_{LUMO}, eV), were calculated. The energy gap (ΔE, eV), global hardness (η, eV), global softness (σ, eV^{-1}), electronegativity (χ, eV), and the amount of electron transfer from the inhibitor molecule to the iron surface (ΔN) were computed using the following Eqs. (5)–(9).

$$\Delta E = E_{LUMO} - E_{HOMO} \tag{5}$$

$$\eta = \frac{E_{LUMO} - E_{HOMO}}{2} \tag{6}$$

Table 3
Analytical Methods and Measured Data.

Method	Measured Data
Cation Chromatography (Cation IC)	Amine concentration in solvent
Anion Chromatography (Anion IC)	Concentrations of HSS anions
Inductively Coupled Plasma-Mass Spectrometry (ICP-MS)	Metal ion concentrations
Gas Chromatography-Mass Spectrometry (GC–MS)	Degradation products in solvent
Scanning Electron Microscopy (SEM)	Surface morphology of corroded samples
X-ray Diffraction (XRD)	Crystalline phases of corrosion products

Table 2
Composition of the Q235 carbon steel sheets used in this study, wt.%.

Element	C	Si	Mn	Cr	Mo	Ni	Cu	V	P	S	Fe
Percentage	0.20	0.30	0.83	0.20	0.11	0.18	0.23	0.005	0.040	0.050	Bal

Fig. 3. Hydrothermal synthesis autoclave and oven for immersion corrosion experiment.

$$\sigma = \frac{1}{\eta} \tag{7}$$

$$\chi = -\frac{E_{HOMO} + E_{LUMO}}{2} \tag{8}$$

$$\Delta N = \frac{\chi_{Fe} - \chi_{inh}}{2(\eta_{Fe} + \eta_{inh})} \tag{9}$$

Herein, χ_{Fe} and η_{Fe} represent the absolute electronegativity and global hardness of iron in eV, respectively. For bulk iron, theoretically, $\chi_{Fe} = 7eV, \eta_{Fe} = 0$ [51]。 χ_{inh} and η_{inh} correspond to the absolute electronegativity and global hardness of the inhibitor molecule in eV, respectively.

To gain a better understanding of the adsorption behavior of mixed corrosion inhibitors on iron surfaces, MD simulations were performed using the Forcite module in Materials Studio 2020. The interaction between inhibitor molecules and the iron surface was modeled within a three-dimensional periodic boundary condition box. Fe (110) surface was cleaved from an iron crystal using the surface builder module and expanded into a 10 × 10 supercell. To simulate the MEA solution used in immersion corrosion experiments and further analyze the synergistic mechanism of the inhibitors, a liquid-phase absorber model was built using the Amorphous Cell module. The iron slab and the liquid-phase model were combined into a simulation box, and a 40 Å vacuum layer was constructed between the iron surface and the solution to ensure that the non-bonded interactions of adsorbates do not interfere with the periodic influence of the underlying surface atoms. The bottom five layers of iron atoms were frozen to disregard minor thermal vibrations. The Forcite calculation task was set to dynamics, employing the COMPASS II force field and the NVT ensemble at 100 °C, with a total simulation time of 500 ps and timestep of 0.5 fs. Detailed MD calculation parameters and geometric configurations can be found in the Supplementary Material.

The formula for calculating the adsorption energy is shown in Eq. (10) [45,52]:

$$E_{ads} = E_{total} - (E_{sur+sol} + E_{inh+sol}) + E_{sol} \tag{10}$$

herein, E_{ads} represents the interaction energy between the inhibitor molecules and the Fe (110) surface in kcal/mol. E_{total} refers to the total energy of the Fe (110) surface with the adsorbed inhibitor molecules and the organic amine absorbent.$E_{sur+sol}$ represents the total energy of the Fe (110) surface and the absorbent without the inhibitor. $E_{inh+sol}$ represents the energy of the absorbent with the added inhibitors. E_{sol} represents the energy of the absorbent without the inhibitor.

3. Results and discussion

3.1. Inhibitor formula screening experiment

To determine the most effective combination for inhibiting both degradation and corrosion, three selected amino acids and three salts were paired in combinations. The molar ratio of the two inhibitors was set at 1:1, with a total concentration of 2000 ppm added to the absorbent. The inhibition performance of these combinations was measured and compared to identify the most suitable pair. As shown in Fig. 4, compared to the degradation rate of 35.79 % and a corrosion rate of 0.155 mmpy for MEA without inhibitors after 10 days, all nine inhibitor combinations exhibited varying degrees of degradation and corrosion inhibition effects. Notably, the combinations of L-MET with the three salts demonstrated outstanding corrosion inhibition efficiency, with a 10-day corrosion rate of approximately 0.005 mmpy and an inhibition efficiency of 97 %. The combinations involving L-ARG also showed significant reductions in corrosion rates, all below 0.155 mmpy, while L-CYS exhibited the least effective corrosion inhibition among the three organic inhibitors.

Similarly, the combinations of L-MET displayed lower degradation rates compared to L-CYS and L-ARG. Among these, the combination of L-MET with PST showed the best inhibition effect, resulting in a degradation rate of only 13.36 % for the MEA solution over 10 days, with a degradation inhibition rate of 62.7 %. Therefore, among the nine tested combinations, the PST + L-MET combination was selected for further validation and optimization studies due to its superior overall performance.

Furthermore, the accumulation of HSS anions over 10 days for different inhibitor combinations is shown in Fig. 5. The PST + L-MET combination continued to exhibit the lowest total HSS concentration, approximately 5475 ppm. Compared to blank MEA solution, the reductions in oxidative degradation products such as glycolate, acetate, and formate were the most significant, while sulfate concentration showed a slight increase. This was attributed to the presence of sulfur in the L-MET, which was oxidized to form sulfate. The same is true for the L-CYS system, where sulfate ions were particularly abundant. In contrast, the L-ARG and Blank absorbent systems, which did not introduce additional sulfur, had sulfate ions primarily originating from the dissolution and oxidation of sulfur contained in carbon steel, with concentrations an order of magnitude lower.

Excluding sulfate, the formation pathways for the other four HSS ions are illustrated in Fig. 6. According to Vevelstad et al.'s calculations, the Gibbs free energies for the reactions producing vinyl alcohol and α-amino-acetaldehyde are −6 kcal and −75 kcal, respectively [53],

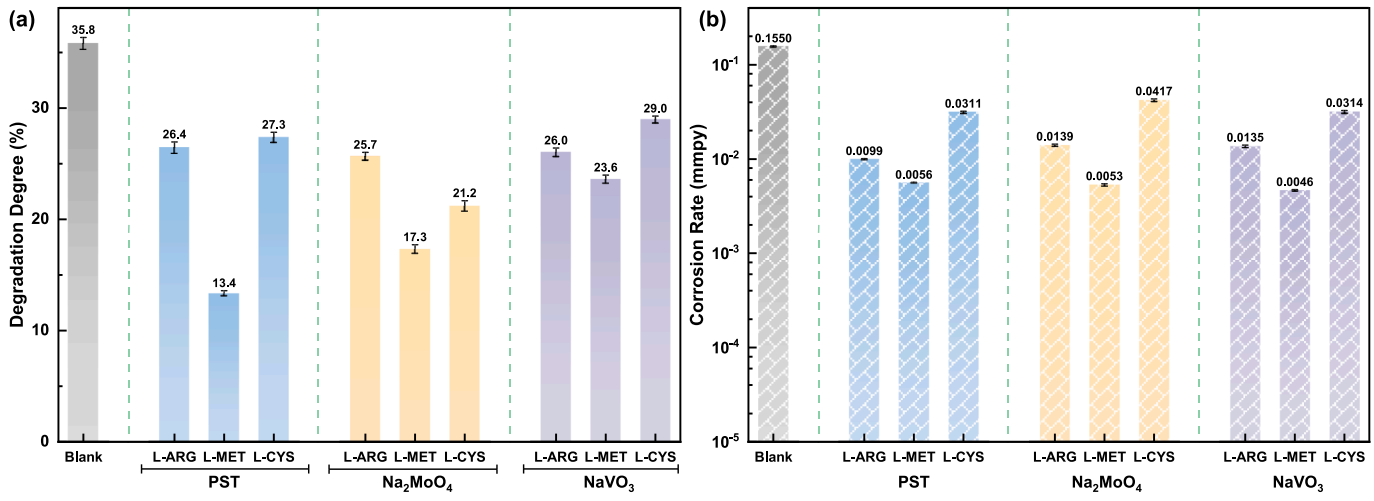

Fig. 4. Degradation degrees (a) and corrosion rates (b) over 10 days for different inhibitor combinations.

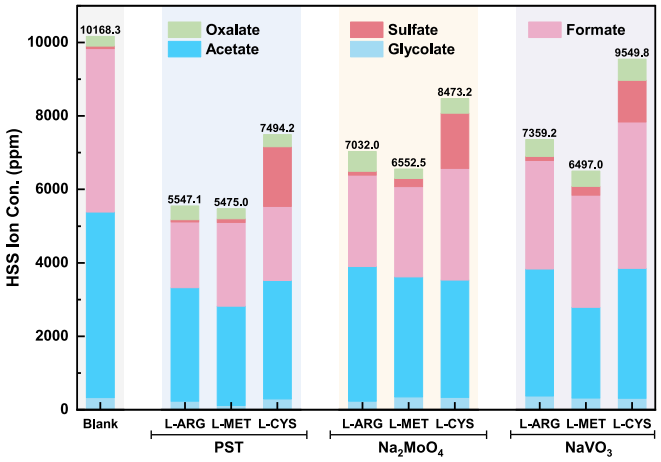

Fig. 5. HSS Accumulation Over 10 Days for Different Inhibitor Combinations.

making the latter reaction more favorable. Consequently, the reaction pathways leading to glycolate and formate dominate, with glycolate being an intermediate of oxalate, which readily decomposes into formate due to its instability. However, the measured concentration of acetate in this experiment was the highest, possibly due to the catalytic effect of Fe^{2+} on the oxidation process, which alters the activation energies of these reactions [14]. Additionally, the dissolution and mass transfer of O_2 in the solution may have limited the formation of α-amino-acetaldehyde to some extent [54].

By correlating the total HSS accumulation with corrosion rates across different inhibitor systems, a positive relationship can be observed. The HSS accumulation reflects the extent of oxidative degradation in the solution, highlighting the complex and interlinked nature of degradation and corrosion.

To compare the effectiveness of the PST + L-MET formulation with individual inhibitors, degradation and corrosion experiments were conducted by adding each of the six selected inhibitors separately to the MEA solution, and the results are shown in Fig. 7. PST + L-MET continued to exhibit the most effective overall inhibition of degradation and corrosion. It is noteworthy that, except for L-CYS, the degradation levels for single inhibitor additions were all below 20 %, lower than those of most composite inhibitors shown in Fig. 4. This suggests that in organic amine absorbent systems, the combination of two inhibitors might result in less effective degradation resistance compared to using one inhibitor alone, implying that random mixing may not necessarily lead to a synergistic effect and could even accelerate degradation.

In terms of corrosion inhibition, the addition of single inhibitors showed a significant improvement over the blank group. Among them, L-ARG demonstrated the best corrosion inhibition effect. When used individually, PST and L-MET achieved corrosion inhibition rates of 81 % and 91 %, respectively. However, when combined, their corrosion inhibition efficiency increased to 96.4 %, which was significantly higher than when used separately.

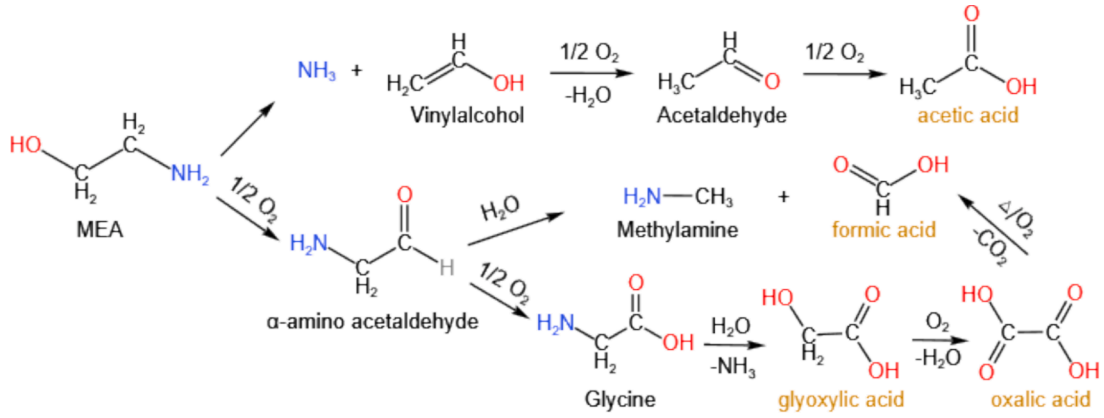

Fig. 6. MEA oxidative degradation pathways leading to the formation of different HSS anions [55].

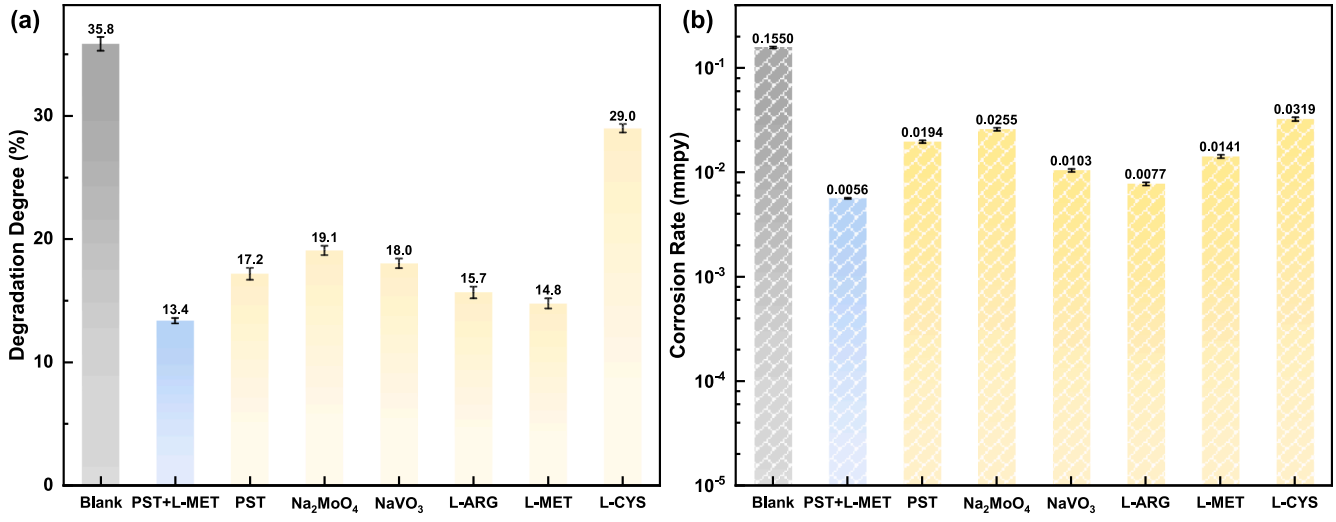

Fig. 7. Comparison of degradation degrees (a) and corrosion rates (b) over 10 days for single inhibitors.

For PST and L-MET used in this study, previous research has suggested several mechanisms for their inhibition. These include self-oxidation, where they sacrifice themselves to protect the amine from degradation; reacting with metal ions in the solution to block their catalytic activity in oxidation reactions and inhibit corrosion; and salting out O_2 to reduce dissolved O_2 concentration, thereby slowing oxidation degradation [56,57].

However, these explanations are insufficient to explain the enhanced degradation and corrosion inhibition effects observed when PST and L-MET are combined. Some studies proposed that the addition of salts could increase the ionic strength of the solution, promoting changes in the solvent molecular structure. This leads to the formation of a stabilized solvation shell that is unfavorable for free radical reactions. These mechanisms indicate that even stable and less easily oxidized salts can effectively inhibit oxidative degradation [58]. Furthermore, there may be a synergistic adsorption mechanism and effect on the carbon steel surface, where larger molecules preferentially adsorb onto the Fe(110) surface, forming a thin film with voids, which are then filled by the other inhibitor molecules to create a bilayer film [45]. According to solvation shell theory and bilayer composite adsorption theory, the inhibition effects will vary with the concentration and ratio of the two inhibitor molecules, and there exists an optimal value that maximizes the synergistic effect.

3.2. Optimal inhibitor concentration screening experiment

Many inhibitors can effectively suppress the oxidative degradation of amines within a specific concentration range. However, at insufficient or excessive concentrations, these additives may actually increase amine degradation [59]. Therefore, before exploring the optimal ratio of the inhibitor system, it is essential to determine the optimal concentration range of the additives. As shown in Fig. 8, significant differences in degradation and corrosion were observed at molar ratio of 1:1 and total concentrations of 2000, 4000, and 8000 ppm. The best degradation inhibition was achieved at a concentration of 4000 ppm, although the corrosion rate was slightly higher than at 2000 ppm. Clearly, a concentration of 8000 ppm had adverse effects on both degradation and corrosion inhibition. Thus, maintaining the concentration within the range of 2000–4000 ppm in the MEA absorbent ensures optimal inhibition performance.

ICP-MS analyzed results of the metal ion concentrations in the liquid samples from corrosion experiments with different inhibitor concentrations are shown in Table 4. It was found that the blank sample, which contained more iron-containing precipitates, had the lowest concentration of dissolved Fe ions, at only 127.3 ppm. However, such precipitates in actual industrial operations can adversely affect the mass and heat transfer processes of the absorbent and cause a series of operational issues when deposited on key equipment. The blank solution was a deep brownish-yellow, while the absorbent with added inhibitors was a lighter yellow. Notably, the absorbent with 8000 ppm inhibitors also had some precipitates, with Fe ion concentrations reaching 250 ppm. In contrast, the absorbents with 2000 and 4000 ppm inhibitors were clearer and more transparent, without insoluble precipitates observed. The Fe ion concentration at 4000 ppm was slightly lower than at 2000 ppm, further demonstrating better inhibition performance. Therefore, in the subsequent optimization experiments, 4000 ppm inhibitors were selected.

3.3. Formula ratio optimization

Degradation and corrosion experiments were conducted with PST and L-MET additive ratios ranging from 1:4 to 4:1, as shown in Fig. 9 and Table 5. Overall, when the ratios of PST to L-MET were between 2:1 and 1:2, both the degradation and corrosion rates maintained at a low level. Specifically, within this range, the degradation inhibition rates exceeded 65 %, with the 14-day degradation level being comparable to that observed after 4 days without inhibitors. The corrosion inhibition

Table 4
Metal Ions in corrosion experiment solvents tested by ICP-MS.

Concentration (ppm)	Fe 56 Helium KED (ppm)	Ni 60 Helium KED (ppm)	Cu 63 Helium KED (ppm)	Static solvent
Blank	127.293*	0.171	0.362	
2000	188.322	0.148	0.277	
4000	181.017	0.123	0.276	
8000	249.559*	0.158	0.188	

* : Flake-like black-brown precipitates in the bottom of the solution

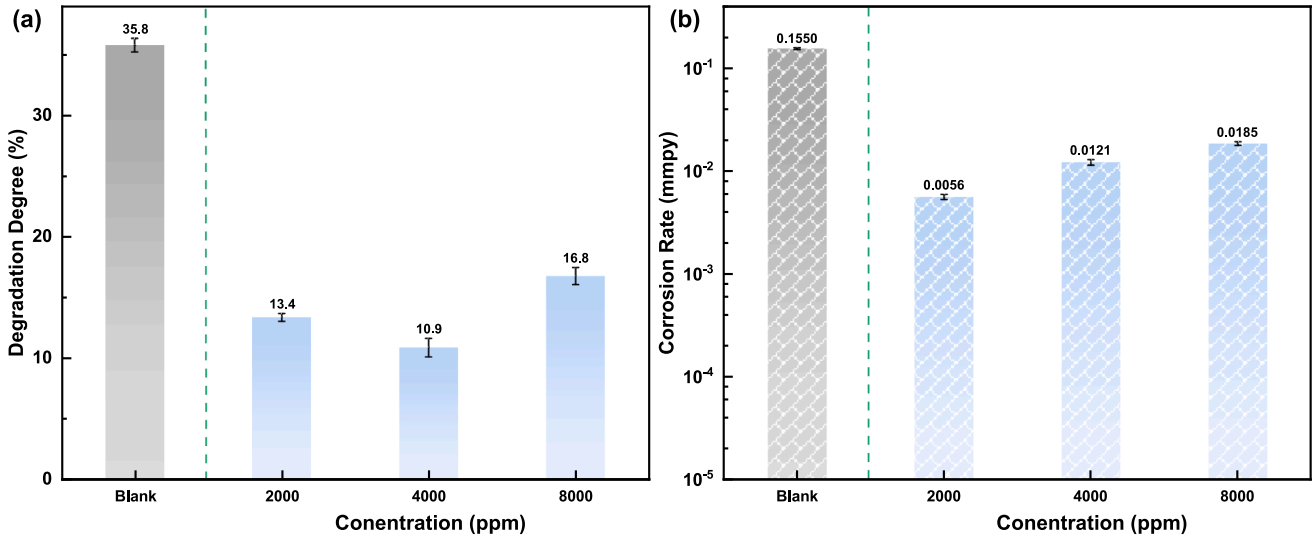

Fig. 8. Comparison of degradation degrees (a) and corrosion rates (b) of composite inhibitors at different concentrations over 10 days at 1:1 addition ratio.

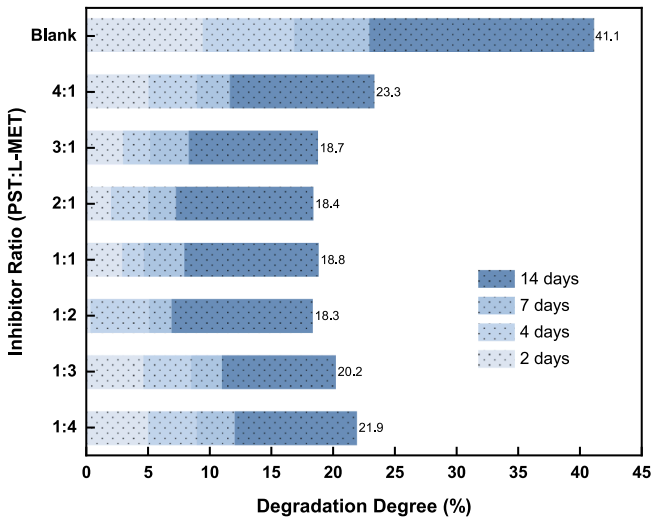

Fig. 9. Comparison of degradation degree of PST + L-MET (4000 ppm) system at different ratio over 14 days.

efficiency at ratio 1:2 reached as high as 98.8 %, demonstrating optimal performance. It is worth noting that when the total inhibitor concentration was controlled at 4000 ppm, all ratios exhibited low degradation levels in the degradation experiments Similarly, the corrosion rate of carbon steel is strongly reduced for all the ratios except the ratio of 1:3.

The HSS accumulation after 14 days of degradation for different inhibitor ratios was further measured, with the results shown in Fig. 10 (a). Consistent with the degradation and corrosion rates, the HSS concentration in the absorber system remained low in the 1:2 to 3:1 ratio range. In particular, the main degradation products, acetate and formate, which are important indicators for evaluating degradation levels, were significantly reduced. The sulfate concentration showed a slight increase due to the addition of L-MET. As for glycolate and oxalate formation, the 2:1 ratio exhibited the highest inhibition effect. Overall, an excess of either PST or L-MET resulted in an increase in total HSS concentration.

The accumulation of neutral degradation products in the absorber is another indicator of degradation. Due to the limitations of the GC–MS instrument, the use of dichloromethane extraction resulted in the loss of some degradation products. Consequently, only pyrazine-type degradation products, which have higher solubility in the organic phase, were detected. Since the degradation experiment lasted only 14 days, more complex downstream products, such as ethylpyrazine or dimethylpyrazine, were not observed; only pyrazine and methylpyrazine were detected, as shown in Fig. 10(b). Notably, the concentration of pyrazine correlated strongly with both the degradation level and HSS concentration. The 2:1 to 1:2 ratio range exhibited higher inhibition rates, while the formation rate of methylpyrazine was relatively slow, with little variation in accumulation across different ratios. According to the pyrazine formation pathways shown in Fig. 11, the generation of methylpyrazine was limited by the concentrations of both pyrazine and formaldehyde.

3.4. Characterization of corrosion products

When carbon steel surfaces without a passivation film are in an active corrosion state, the corrosion process in the absorbent involves the oxidation of Fe on the surface to Fe ions, generation of electrons, and the reduction reaction in the solution that consumes these electrons. Overall, this redox reaction occurs through the interaction of three elements: the anode, cathode, and electrolyte. Existing corrosion inhibitors generally operate through electrochemical and physico-chemical mechanisms. The electrochemical mechanism delays the corrosion process by interfering with the anodic, cathodic, or both reactions. The physico-chemical mechanism includes physical adsorption (inhibitor molecules are attracted to the metal surface through electrostatic and van der Waals forces) and chemical adsorption (reactive

Table 5
Comparison of the corrosion rates of PST + L-MET at different ratios over 14 days (4000 ppm).

Inhibition Ratio (PST: L-MET)	Blank	4:1	3:1	2:1	1:1	1:2	1:3	1:4
Corrosion Rate (mmpy)	0.1275	0.0792	0.0185	0.0062	0.0058	0.0015	0.1651	0.0313
IE_C (%)		37.88	85.49	95.14	95.45	98.82	−29.49	75.45

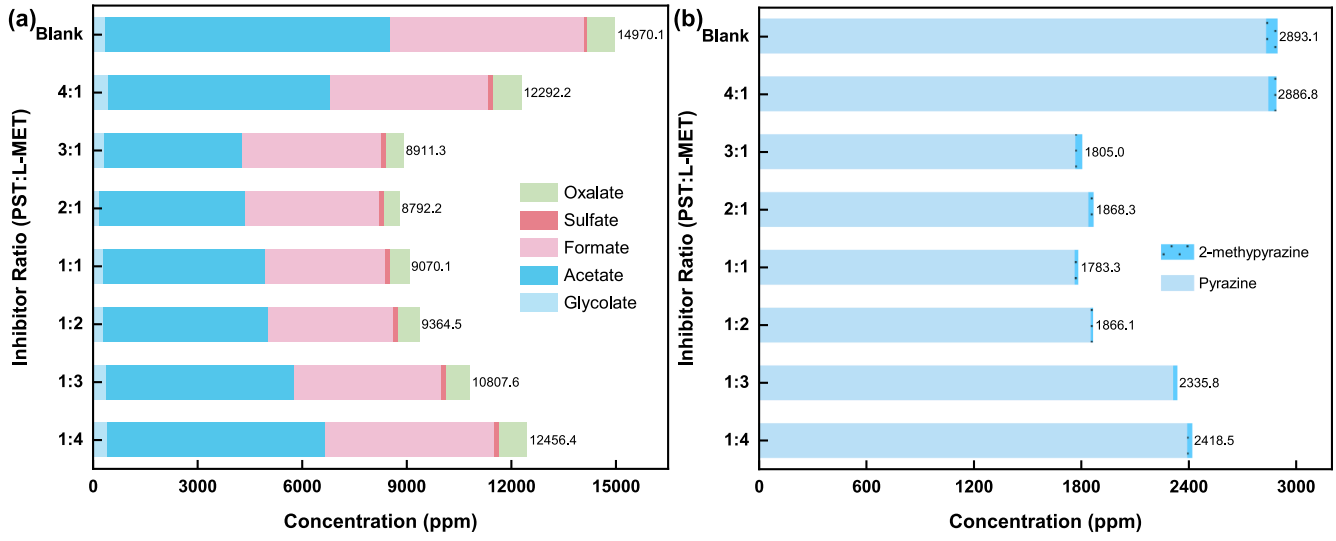

Fig. 10. HSS concentrations (a) and pyrazine product concentrations (b) after 14-day degradation in PST + L-MET system at different ratios (4000 ppm).

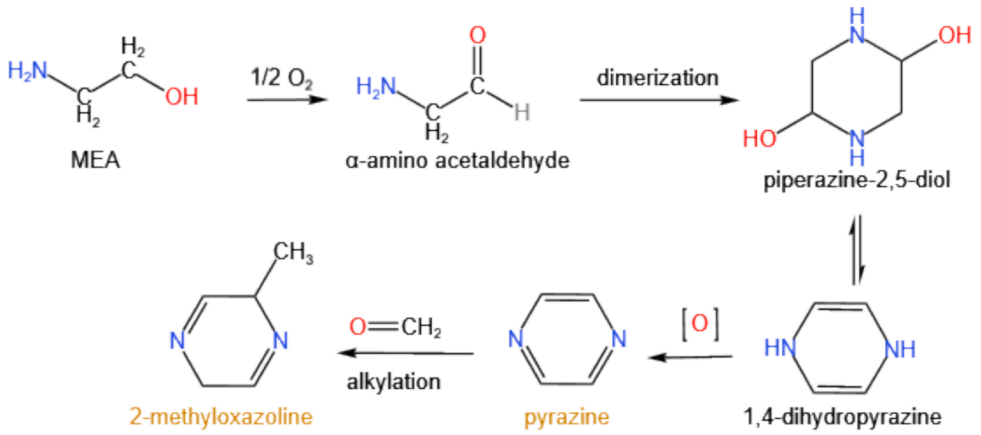

Fig. 11. Formation pathways of pyrazine-type degradation products in MEA absorbent.

groups in the inhibitor transfer to the metal surface and form ligand bonds through interactions such as ion exchange, surface complexation, chelation, and precipitation) [60].

Figs. 12 and 13 show the characterization results of corrosion products on carbon steel sheets in MEA systems with single inhibitors. Only the L-CYS system formed a $FeN_{0.0324}$ iron nitride layer on the carbon steel surface t, but it was cracked and poorly adhesive, thus failing to protect the carbon steel from further corrosion. The other systems did not form a complete protective layer. Instead, numerous pits, a feature of corrosion, were observed on the surface. According to the XRD results, although no protective film was formed on the carbon steel surface in the other systems, small amounts of $FeN_{0.0324}$ iron nitride were detected along with Fe. Experiments by Li et al. have shown that ions like 2-methylimidazole and $K_3[Fe(CN)_6]$ can form iron-based nanocrystals like $FeN_{0.0324}$ under specific high-temperature conditions [61]. Research indicates that the lone pair of nitrogen atoms in the oxidative degradation products of MEA and N-(2-hydroxyethyl)imidazole (HEI) can adsorb synergistically with metals, making them easy to adhere to metal surfaces [62]. Thus, in this system, the deposition of iron nitride on the carbon steel surface may result from the binding of nitrogen-containing compounds like HEI with dissolved Fe ions near the carbon steel surface.

The composition of corrosion products differs significantly among the composite inhibitor systems with varying ratios, as shown in Figs. 14 and 15. According to the XRD results, the corrosion product layer on the carbon steel surface in the 1:3 system exhibits a cluster-like cotton ball structure, primarily composed of siderite and iron nitride. However, this corrosion product layer does not form a good protective and adhesive layer on the carbon steel surface, failing to prevent further corrosion. In the 1:2 system, only Fe crystal plane peaks were detected on the carbon steel surface, but without any deposition of nitrides. For the systems from 4:1 to 1:1 as shown in Fig. 14, a noticeable decrease in surface deposits is observed with the main coverage being $Fe/FeN_{0.0324}$. Although a small amount of iron nitride was detected in the 1:1 system, its presence is minimal compared to the intensity of the Fe peaks, indicating that excessive addition of PST has a negative impact on corrosion resistance.

Table 6 highlights the corrosion product composition in various systems. For systems containing PST or L-MET individually, $FeN_{0.0324}$ became a major component, which was similar to blank system. In contrast, in PST + L-MET systems, especially at the 1:2 ratio, $FeN_{0.0324}$ and $FeCO_3$ were significantly suppressed. This finding suggests that the combination of PST and L-MET effectively blocks the adsorption of nitrogen-containing molecules/ions (e.g., $FeN_{0.0324}$) and carbonate-

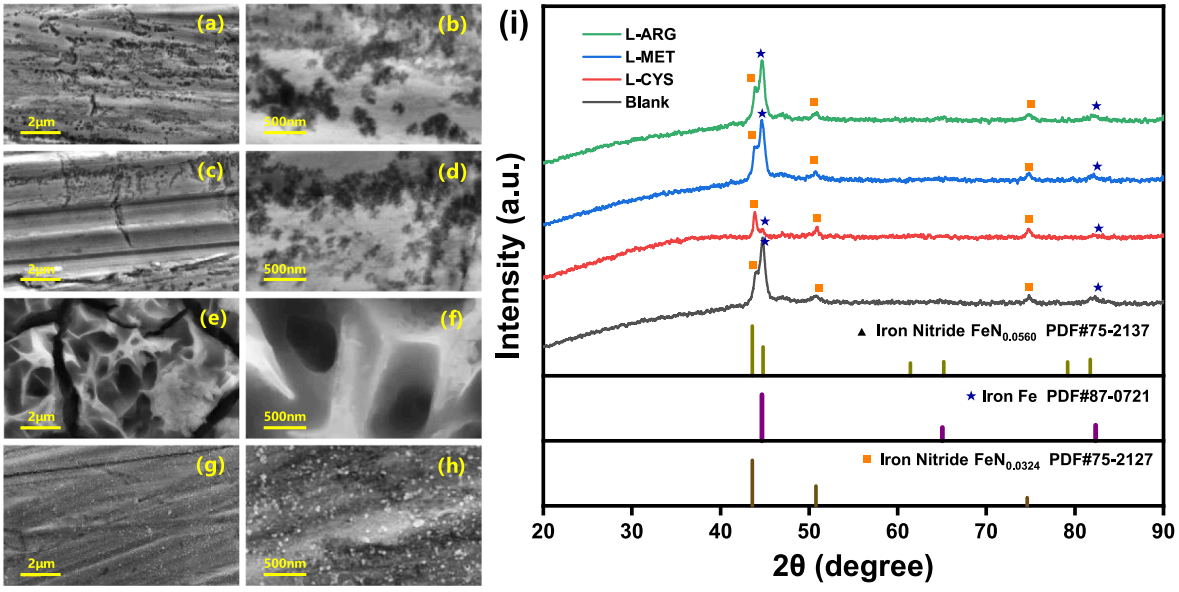

Fig. 12. SEM images [(a), (b): L-ARG; (c), (d): L-MET; (e), (f): L-CYS; (g), (h): Blank] and XRD characterization (i) of corrosion products in MEA systems with single amino acid at 100 °C.

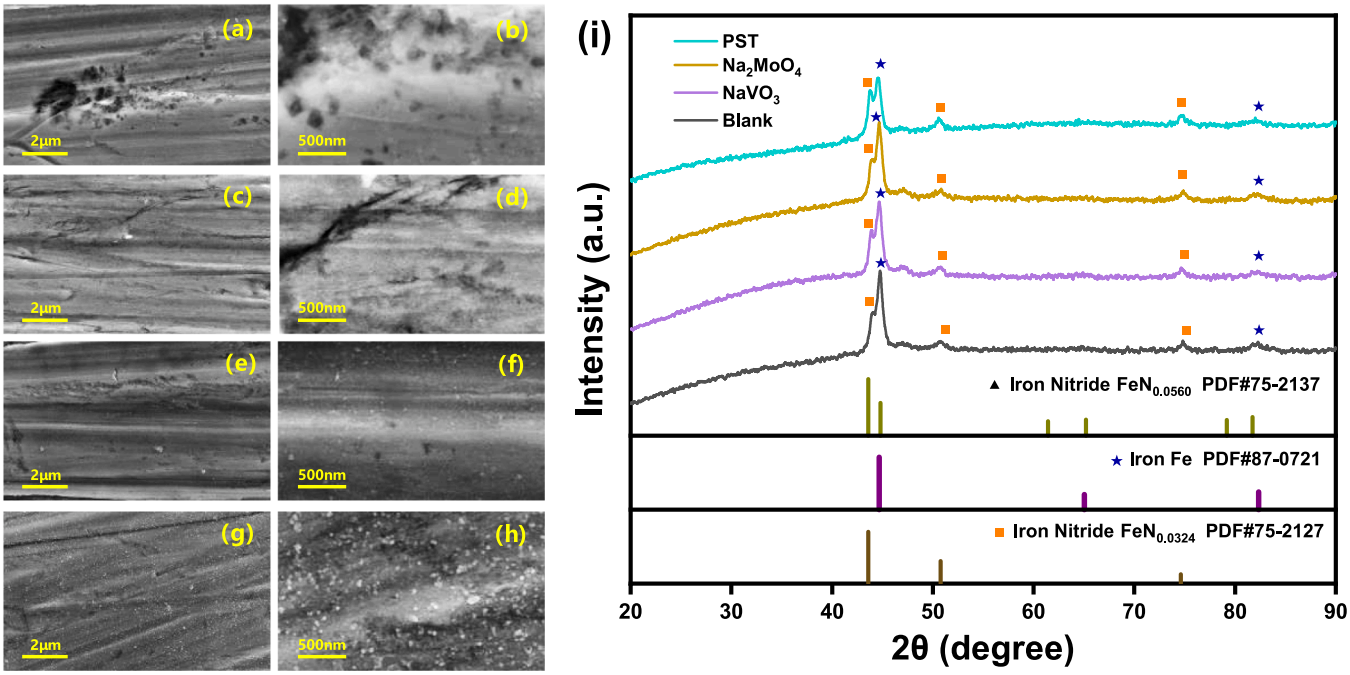

Fig. 13. SEM images [(a), (b): PST; (c), (d): $Na_2 MoO_4$; (e), (f): $NaVO_3$; (g), (h): Blank] and XRD characterization (i) of corrosion products in MEA systems with salt inhibitors at 100 °C.

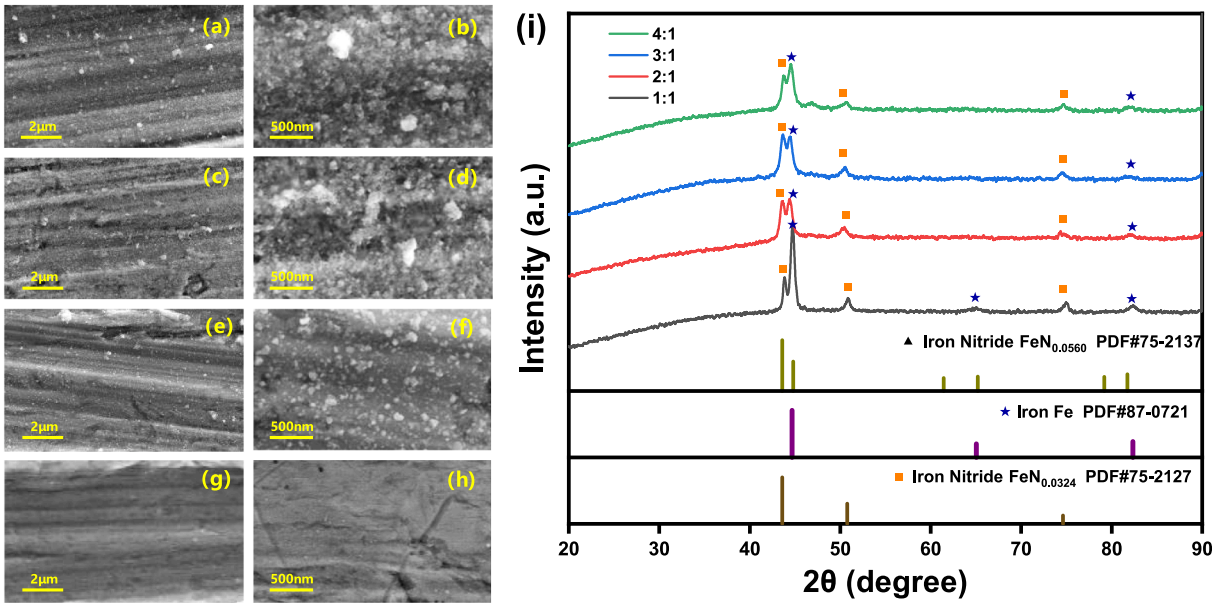

Fig. 14. SEM images [(a), (b): 4:1; (c), (d): 3:1; (e), (f): 2:1; (g), (h): 1:1] and XRD patterns (i) of corrosion products on carbon steel sheets in MEA systems with composite inhibitors at 100 °C.

based ions (e.g., $FeCO_3$) onto the carbon steel surface. As depicted in Fig. 16, this synergistic interaction between PST and L-MET leads to the formation of a denser protective film on the Fe (110) surface. The layer further shields the surface from corrosive species, thereby minimizing the formation of corrosion products and enhancing the overall inhibition performance [63,64].

3.5. DFT calculations

The geometric structures of the inhibitor molecules/ions were optimized using the Dmol3 module, and their highest occupied molecular orbitals (HOMO) and lowest unoccupied molecular orbitals (LUMO) were calculated, as shown in Table 7 and Table 8. According to frontier molecular orbital theory, the electron-donating and electron-accepting abilities are primarily related to the HOMO and LUMO of the molecules [65]. Combined with the electronegativity values (χ) in Table 7, it was evident that L-CYS exhibited superior electron-donating and electron-accepting abilities. Among the salt inhibitors, sodium metavanadate had significantly lower E_{HOMO} and E_{LUMO} values, indicating higher electronegativity. The electron-donating/accepting abilities of L-MET and PST were less prominent.

The energy gap (ΔE) is an important parameter for discussing the reactivity of molecules with metal surfaces; a lower ΔE indicates that the molecule is more easily adsorbed onto the metal surface [66]. Global

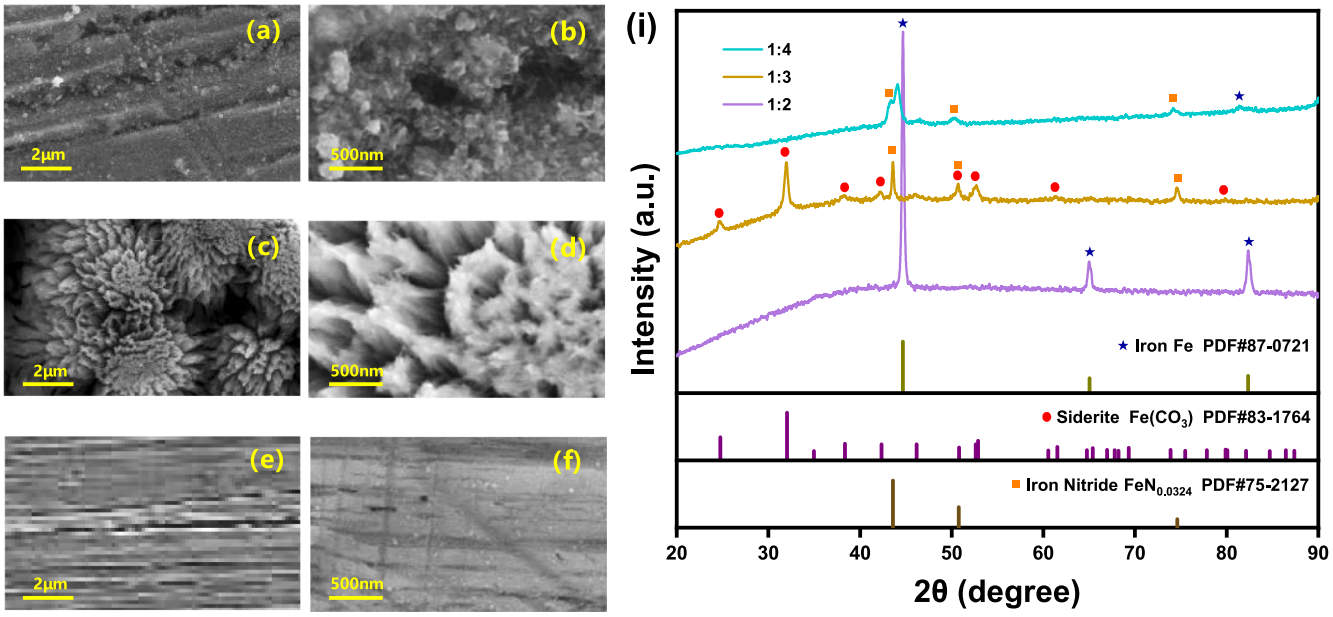

Fig. 15. SEM images [(a), (b): 1:4; (c), (d): 1:3; (e), (f): 1:2] and XRD patterns (i) of corrosion products on carbon steel sheets in MEA systems with composite inhibitors at 100 °C.

Table 6
Summary of corrosion products in different PST + L-MET systems.

System	Blank	PST	L-MET	PST + L-MET System						
				4:1	3:1	2:1	1:1	1:2	1:3	1:4
Fe	++	++	++	++	++	++	++	++		+
$FeN_{0.0324}$	+	++	+	++	++	++	+		+	++
$FeCO_3$									++	

++: The primary detected component; +: The secondary detected component.

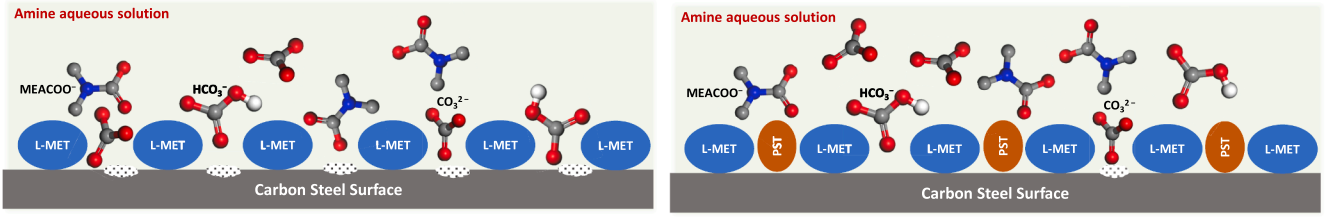

Fig. 16. Schematic of the adsorption film formation by PST and L-MET on carbon steel surface.

Table 7
DFT calculation results.

Inhibitors	E_{LUMO} (eV)	E_{HOMO} (eV)	ΔE (eV)	η (eV)	χ (eV)	ΔN	σ (eV^{-1})
L-MET	−1.191	−5.039	3.848	1.924	3.115	1.010	0.520
L-ARG	−1.279	−5.365	4.087	2.043	3.322	0.900	0.489
L-CYS	−1.550	−5.684	4.134	2.067	3.617	0.818	0.484
PST^{2-}	5.984	3.989	1.995	0.997	−4.986	6.008	1.003
MoO_4^{2-}	8.654	4.411	4.243	2.122	−6.532	3.189	0.471
VO_3^-	1.090	−0.623	1.713	0.857	−0.233	4.222	1.167

softness (σ) is also a key parameter for assessing the likelihood of molecular adsorption on the metal surface; a higher σ value suggests a greater adsorption potential. According to the calculations in Table 7, L-MET, among the organic inhibitors, had the lowest energy gap and the highest σ value, indicating it was more likely to adsorb onto the metal surface. Among the salt inhibitors, the adsorption abilities of tartaric acid and metavanadate are similar.

The electron transfer number (ΔN) typically represents the number of electrons transferred from the inhibitor to the metal during the interaction process [67]. Table 7 shows that all inhibitors have positive ΔN values, indicating that electrons are transferred from the inhibitor to the metal's unoccupied d-orbitals. L-MET and PST exhibited the highest ΔN values among the six inhibitors, respectively, demonstrating that both were highly effective in providing electrons to inhibit corrosion.

Table 8
The optimized structure of inhibitors and distributions of HOMO, LUMO orbitals.

	Structure	HOMO	LUMO
L-MET	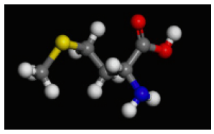	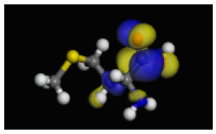	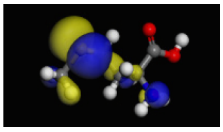
L-ARG	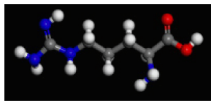	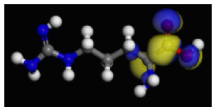	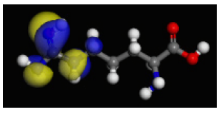
L-CYS	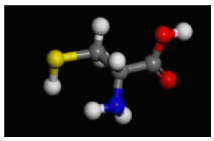	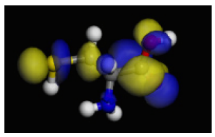	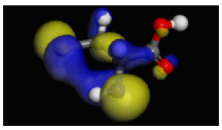
PST^{2-}	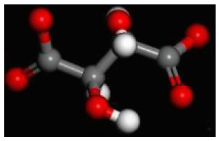	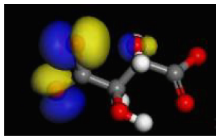	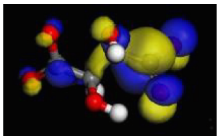
MoO_4^{2-}	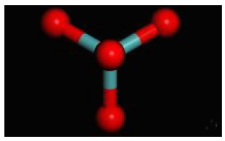	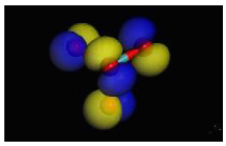	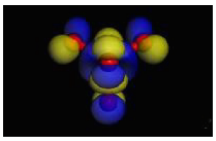
VO_3^-	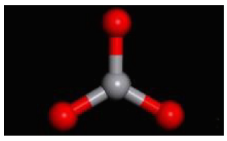	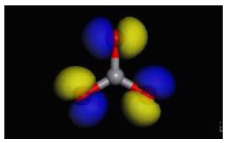	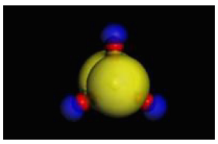

3.6. MD Simulations: Synergistic inhibition mechanisms

The detailed MD simulation processes, as well as the composition of the inhibitor solution systems, are provided in the Supplementary Material. The adsorption equilibrium configurations are shown in Fig. 17, where the top-down view displays molecules adsorbed within 0.15 Å of the Fe (110) surface. Inhibitor molecules adsorbed on the Fe (110) surface, forming an inhibitor film that prevents carbon steel from corroding. Additionally, components in the absorbent such as MEA, $MEAH^+$, $MEACOO^-$, and HCO_3^- also adsorbed onto the Fe (110) surface, further modifying the film's thickness and density. The introduction of L-MET increased the adsorption of both PST and L-MET molecules, enhancing the film's density and coverage while reducing the number of free inhibitor molecules in solution and minimizing voids. When PST was added alone, only one inhibitor molecule adsorbed onto the Fe (110) surface, whereas four molecules adsorbed when only L-MET was used. With a 1:1 PST to L-MET ratio, the number of adsorbed inhibitor molecules increased to seven, and at ratios of 2:1 and 1:2, three and four inhibitor molecules adsorbed, respectively.

Adsorption energy E_{ads} is a key indicator for evaluating the performance of corrosion inhibitors. The greater the absolute value of E_{ads}, the more stable the adsorption configuration and the better the corrosion inhibition performance. E_{ads} for different ratios of the mixed inhibitors interacting with the Fe (110) surface are shown in Table 9. The

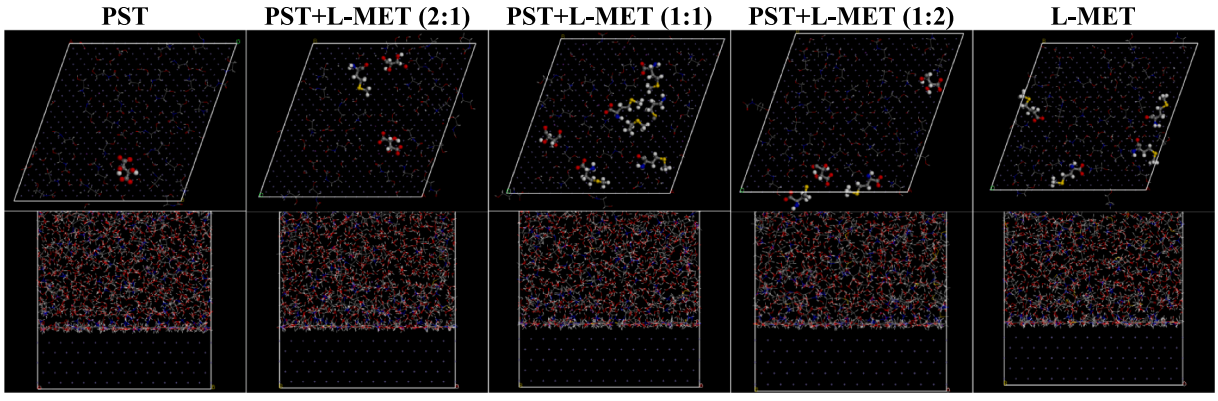

Fig. 17. Equilibrium configurations of mixed corrosion inhibitors adsorbed on the Fe (110) surface in Different Inhibitor-Absorbent Systems.

Table 9
Adsorption Energies of Different Inhibitor Systems.

Systems	E_{total} (kcal/mol)	$E_{sur+sol}$(kcal/mol)	$E_{inh+sol}$ (kcal/mol)	E_{sol} (kcal/mol)	E_{ads} (kcal/mol)
PST	−35407.01	−21093.28	−33411.04	−19216.91	−119.59
PST + L-MET (2:1)	−33476.20	−20534.45	−31496.95	−18793.82	−238.61
PST + L-MET (1:1)	−32870.99	−20039.43	−30868.38	−18579.10	−542.27
PST + L-MET (1:2)	−31738.58	−21561.88	−29692.33	−19831.87	−316.24
L-MET	−29952.33	−22889.64	−27935.59	−21191.03	−318.13

calculation results indicated that the ratio of PST to L-MET affected E_{ads} , suggesting a strong interaction between the inhibitors and the Fe (110) surface, leading to enhanced corrosion inhibition.

It is worth noting that while the MD simulations suggested optimal adsorption energy at a 1:1 ratio, the experimental results showed the lowest corrosion rate at a 1:2 ratio. This discrepancy can be attributed to the limited time scale of the MD simulations, which were conducted over 500 ps without accounting for changes in solution composition. In the simulations, degradation products were not generated, and the dynamic interactions between these products and the inhibitors were not modeled. In contrast, the corrosion experiments involved extended exposure (over 200 h) to high temperatures, leading to solvent degradation and changes in solution composition. These changes could influence the adsorption behavior of inhibitors, ultimately affecting the corrosion rate [52,53].

Despite these differences, the MD simulations clearly demonstrate that the addition of L-MET to PST further reduces adsorption energy, supporting its positive effect on corrosion inhibition. These findings provide valuable insights into the underlying mechanisms of the PST + L-MET system.

The diffusion coefficient is a critical parameter in evaluating the mobility of various corrosive species in solution. When an adsorption film forms on the Fe (110) surface, it can inhibit the diffusion of $MEACOO^-$ and HCO_3^- ions toward the carbon steel surface. The reduction in ion mobility can be attributed to the density, structure, and stability of the inhibitor film, which influences the adsorption strength of each species and their subsequent diffusion rates. The diffusion coefficient is proportional to the slope of the mean square displacement (MSD) versus time curve. Therefore, using the Forcite module, MSD was calculated from the MD simulation trajectory files at 5 fs intervals. The relatively stable regions of the MSD curve were selected for linear fitting to obtain the average diffusion coefficients of $MEACOO^-$ and HCO_3^- in the system. The fitted MSD-time lines for two main corrosive ions, HCO_3^- and $MEACOO^-$, are respectively shown in Fig. 18, and the corresponding equations and diffusion coefficients are presented in Table 10.

As shown in Fig. 18, when the ratios reached 2:1 and 1:1, the MSD curves for HCO_3^- exhibited a relatively lower slope, indicating that diffusion was significantly suppressed, suggesting that it provided stronger resistance to HCO_3^- diffusion. Table 10 further shows that at 1:1 ratio, the diffusion coefficient reached its lowest value, lower than when either inhibitor was used alone, implying that the synergistic interaction. And interestingly, the diffusion behavior of $MEACOO^-$ did not follow the same trend as HCO_3^- across the various inhibitor ratios. At the 1:1 ratio, $MEACOO^-$ exhibited a higher diffusion coefficient (11.29), whereas it decreased significantly at the 2:1 and 1:2 ratios, suggesting that the film's efficiency in blocking $MEACOO^-$ was different from HCO_3^-. $MEACOO^-$ and HCO_3^- ions may experience different degrees of interactions with the inhibitor molecules at certain ratios.

The synergistic effect between PST and L-MET in the 2:1 to 1:2 ratio range indicates that these inhibitors work together to enhance the formation of a more compact and stable film, which significantly reduces the mobility of both HCO_3^- and $MEACOO^-$. The calculation results are in good agreement with the experimental findings, supporting the same optimal ratio range. The combination of these inhibitors likely results in an optimized surface coverage, where PST provides strong electrostatic adsorption, and L-MET contributes to the film's cohesion and stability through its ability to interact with both the surface and the corrosive ions. The reduction in free inhibitor molecules in solution, further suggests that more inhibitor molecules are adsorbed onto the Fe (110) surface, contributing to the denser inhibitor film.

It is important to note that these MD simulations were conducted over a limited timescale and didn't account for the potential impact of long-term degradation products, such as HSSs, which could influence the diffusion and corrosion behavior over time. Future studies should aim to extend the simulation duration and incorporate degradation products to capture the long-term impact more accurately on inhibitor performance.

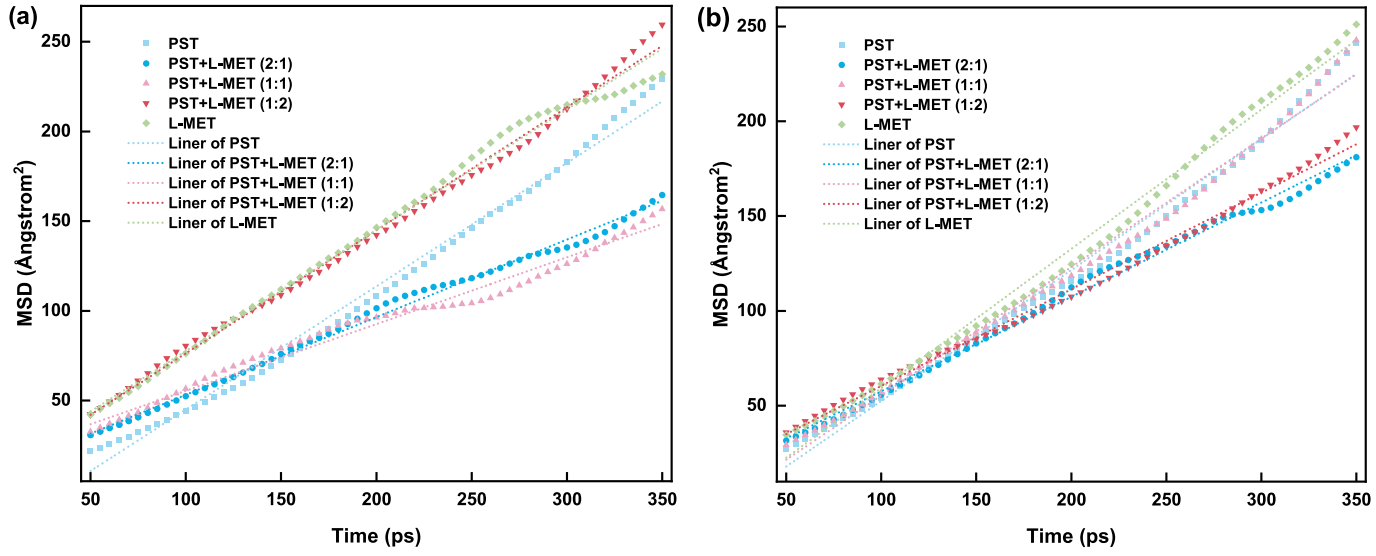

Fig. 18. The relationship between the MSD of HCO_3^-(a), $MEACOO^-$(b) and time in different systems.

Table 10
The average diffusion coefficients of HCO_3^- and $MEACOO^-$ in different systems.

Ion type	Systems	Fitting equation	R^2	Average diffusion coefficient ($10^{-6}cm^2/s$)
HCO_3^-	**PST**	MSD = 0.7002 t − 27.035	0.9921	11.67
	PST + L-MET (2:1)	MSD = 0.4304 t + 10.536	0.9952	7.17
	PST + L-MET (1:1)	MSD = 0.3659 t + 19.802	0.9808	6.10
	PST + L-MET (1:2)	MSD = 0.687 t + 7.4154	0.9958	11.45
	L-MET	MSD = 0.6697 t + 11.262	0.9925	11.16
$MEACOO^-$	**PST**	MSD = 0.6903 t − 16.541	0.9904	11.51
	PST + L-MET (2:1)	MSD = 0.4977 t + 7.9113	0.9952	8.30
	PST + L-MET (1:1)	MSD = 0.6772 t − 12.31	0.9906	11.29
	PST + L-MET (1:2)	MSD = 0.5093 t + 9.6147	0.9948	8.49
	L-MET	MSD = 0.7341 t − 14.106	0.9921	12.24

4. Conclusion

This study investigated the synergistic effects of composite inhibitors on degradation and corrosion in MEA systems for CO_2 capture. By integrating six inhibitors, the research demonstrated that a 2:1 to 1:2 ratio range of PST and L-MET are optimal inhibitors preventing both corrosion and degradation. Additionally, improper inhibitor ratios may deteriorate the film's protective capabilities. MD simulations and quantum chemical calculations further confirmed that PST and L-MET forms a stable bilayer adsorption film on the Fe (110) surface, minimizing adsorption energy and corrosion rates. Additionally, the diffusion coefficients in different systems indicated that the optimal ratio range significantly suppressed ion mobility, which correlated with the observed enhancement in corrosion resistance.

These findings have significant practical implications. As biodegradable and environmentally friendly inhibitors, PST and L-MET support sustainability goals and reduce regulatory compliance costs due to their low toxicity and environmental impact. The use of PST and L-MET as inhibitors can prolong the operational lifespan of CO_2 capture systems and lower costs by reducing solvent degradation and corrosion-related maintenance.

This study also acknowledges certain limitations. Notably, the stability of the inhibitors was not tested due to the challenges in quantitatively assessing the inhibitors over extended periods. Future work should address this by incorporating stability tests and extending the simulation and experimental timescales to fully capture the degradation dynamics and long-term efficiency of the inhibitors.

CRediT authorship contribution statement

Yuwei Wang: Conceptualization, Investigation, Methodology, Formal analysis, Visualization, Software, Writing – original draft. **Mengxiang Fang:** Resources, Supervision, Writing – review & editing, Funding acquisition. **Jiabao Yi:** Funding acquisition, Investigation, Methodology. **Hai Yu:** Methodology, Writing – review & editing. **Qi Yang:** Conceptualization, Investigation, Validation. **Xiaozheng Lu:** Data curation, Formal analysis, Validation. **Tao Wang:** Funding acquisition, Resources, Supervision.

Declaration of competing interest

The authors declare that they have no known competing financial interests or personal relationships that could have appeared to influence the work reported in this paper.

Acknowledgment

This work is supported by National Key R&D Program of China (2023YFE0199300), Pioneer R&D Program of Zhejiang Province-China (2022C03040) and the Fundamental Research Funds for the Central Universities (2022ZFJH04).

Appendix A. Supplementary material

Supplementary data to this article can be found online at https://doi.org/10.1016/j.seppur.2025.131712.

Data availability

Data will be made available on request.

References

[1] V. Buvik, K.K. Høisæter, S.J. Vevelstad, H.K. Knuutila, A review of degradation and emissions in post-combustion CO_2 capture pilot plants, Int. J. Greenh. Gas Control 106 (2021), https://doi.org/10.1016/j.ijggc.2020.103246.
[2] A. Manuilova, J. Koiwanit, L. Piewkhaow, M. Wilson, C.W. Chan, P. Tontiwachwuthikul, Life cycle assessment of post-combustion CO_2 capture and CO_2- enhanced oil recovery based on the boundary dam integrated carbon capture and storage demonstration project in saskatchewan, Energy Procedia 63 (2014) 7398–7407, https://doi.org/10.1016/j.egypro.2014.11.776.
[3] A.K. Morken, S. Pedersen, E.R. Kleppe, A. Wisthaler, K. Vernstad, Ø. Ullestad, N. E. Flø, L. Faramarzi, E.S. Hamborg, Degradation and emission results of amine plant operations from MEA testing at the CO_2 technology centre mongstad, Energy Procedia 114 (2017) 1245–1262, https://doi.org/10.1016/j.egypro.2017.03.1379.
[4] S. Dhingra, P. Khakharia, A. Rieder, A. Cousins, A. Reynolds, J. Knudsen, J. Andersen, R. Irons, J. Mertens, M.A. Zahra, P. Van Os, E. Goetheer, Understanding and modelling the effect of dissolved metals on solvent degradation in post combustion CO_2 capture based on pilot plant experience, Energies 10 (2017), https://doi.org/10.3390/en10050629.
[5] I. Aouini, A. Ledoux, L. Estel, S. Mary, J. Grimaud, B. Valognes, Study of carbon dioxide capture from industrial incinerator flue gas on a laboratory scale pilot, Energy Procedia 4 (2011) 1729–1736, https://doi.org/10.1016/j.egypro.2011.02.047.
[6] A.B. Rao, E.S. Rubin, A technical, economic, and environmental assessment of amine-based CO_2 capture technology for power plant greenhouse gas control, Environ. Sci. Technol. 36 (2002) 4467–4475, https://doi.org/10.1021/es0158861.
[7] C. Gouedard, D. Picq, F. Launay, P.L. Carrette, Amine degradation in CO_2 capture. I. a review, Int. J. Greenh. Gas Control 10 (2012) 244–270, https://doi.org/10.1016/j.ijggc.2012.06.015.
[8] Q. Huang, J. Thompson, S. Bhatnagar, P. Chandan, J.E. Remias, J.P. Selegue, K. Liu, Impact of flue gas contaminants on monoethanolamine thermal degradation, Ind. Eng. Chem. Res. 53 (2014) 553–563, https://doi.org/10.1021/ie403426c.
[9] G. Léonard, D. Toye, G. Heyen, Experimental study and kinetic model of monoethanolamine oxidative and thermal degradation for post-combustion CO_2 capture, Int. J. Greenh. Gas Control 30 (2014) 171–178, https://doi.org/10.1016/j.ijggc.2014.09.014.
[10] S.A. Bedell, Amine autoxidation in flue gas CO_2 capture-Mechanistic lessons learned from other gas treating processes, Int. J. Greenh. Gas Control 5 (2011) 1–6, https://doi.org/10.1016/j.ijggc.2010.01.007.
[11] I. Eide-Haugmo, Environmental impacts and aspects of absorbents used for CO_2 capture, Dep. Chem. Eng. (2011) 365.
[12] S.A. Bedell, Oxidative degradation mechanisms for amines in flue gas capture, Energy Procedia 1 (2009) 771–778, https://doi.org/10.1016/j.egypro.2009.01.102.
[13] L. Braakhuis, H.K. Knuutila, Predicting solvent degradation in absorption–based CO_2 capture from industrial flue gases, Chem. Eng. Sci. 279 (2023) 118940, https://doi.org/10.1016/j.ces.2023.118940.
[14] S. Chi, G.T. Rochelle, Oxidative degradation of monoethanolamine, Ind. Eng. Chem. Res. 41 (2002) 4178–4186, https://doi.org/10.1021/ie010697c.
[15] A.K. Voice, G.T. Rochelle, Inhibitors of monoethanolamine oxidation in CO_2 capture processes, Ind. Eng. Chem. Res. 53 (2014) 16222–16228, https://doi.org/10.1021/ie500996z.
[16] A.J. Sexton, G.T. Rochelle, Catalysts and inhibitors for oxidative degradation of monoethanolamine, Int. J. Greenh. Gas Control 3 (2009) 704–711, https://doi.org/10.1016/j.ijggc.2009.08.007.
[17] A. Jaffer, D. Fulmer, J. Ensslen, Recent developments in organic oxygen scavenger technology, NACE - Int Corros. Conf. Ser. (2006) 066871–0668712.
[18] S.P.J.N. Senanayake, P.K.J.P.D. Wanasundara, F. Shahidi, Antioxidants: science, technology, and applications, Bailey's Ind. Oil Fat Prod. (2020) 1–61, https://doi.org/10.1002/047167849x.bio002.pub2.
[19] G.S. Goff, G.T. Rochelle, Oxidation inhibitors for copper and iron catalyzed degradation of monoethanolamine in CO_2 capture processes, Ind. Eng. Chem. Res. 45 (2006) 2513–2521, https://doi.org/10.1021/ie0490031.

[20] C.H. Blachly, H. Ravner, Stabilization of Monoethanolamine Solutions in Carbon Dioxide Scrubbers, J. Chem. Eng. Data 11 (1966) 401–403, https://doi.org/10.1021/je60030a033.

[21] J. Elnan, Screening of Inhibitors for Amine Degradation, (2012).

[22] R. Idem, P. Tontiwachwuthikul, C. Saiwan, T. Supap, P. Pitipuech, Method for inhibiting amine degradation during co2 capture from a gas stream, (2013). http://www.google.com/patents/CA2644088C?cl=en.

[23] L. Zheng, Corrosion behavior of carbon steel in piperazine solutions for post-combustion CO_2 capture, ECS Meet. Abstr. (2014) 497, https://doi.org/10.1149/ma2014-01/7/497. MA2014-01.

[24] Y. Sun, J.E. Remias, J.K. Neathery, K. Liu, Electrochemical study of corrosion behaviour of carbon steel A106 and stainless steel 304 in aqueous monoethanolamine, Corros. Eng. Sci. Technol. 46 (2011) 724–731, https://doi.org/10.1179/1743278210Y.0000000001.

[25] N. Zhang, D. Zeng, G. Xiao, J. Shang, Y. Liu, D. Long, Q. He, A. Singh, Effect of Cl-accumulation on corrosion behavior of steels in H_2S/CO_2 methyldiethanolamine (MDEA) gas sweetening aqueous solution, J. Nat. Gas Sci. Eng. 30 (2016) 444–454, https://doi.org/10.1016/j.jngse.2016.02.055.

[26] J. Gao, S. Wang, C. Sun, B. Zhao, C. Chen, Corrosion behavior of carbon steel at typical positions of an amine-based CO_2 capture pilot plant, Ind. Eng. Chem. Res. 51 (2012) 6714–6721, https://doi.org/10.1021/ie203045v.

[27] L. Zheng, J. Landon, W. Zou, K. Liu, Corrosion benefits of piperazine as an alternative CO_2 capture solvent, Ind. Eng. Chem. Res. 53 (2014) 11740–11746, https://doi.org/10.1021/ie501346z.

[28] L. Zheng, N.S. Matin, J. Thompson, J. Landon, N.E. Holubowitch, K. Liu, Understanding the corrosion of CO_2-loaded 2-amino-2-methyl-1-propanol solutions assisted by thermodynamic modeling, Int. J. Greenh. Gas Control 54 (2016) 211–218, https://doi.org/10.1016/j.ijggc.2016.09.005.

[29] K.B. Fischer, A. Daga, D. Hatchell, G.T. Rochelle, MEA and piperazine corrosion of carbon steel and stainless steel, Energy Procedia 114 (2017) 1751–1764, https://doi.org/10.1016/j.egypro.2017.03.1303.

[30] B. Zhao, Y. Sun, Y. Yuan, J. Gao, S. Wang, Y. Zhuo, C. Chen, Study on corrosion in CO_2 chemical absorption process using amine solution, Energy Procedia 4 (2011) 93–100, https://doi.org/10.1016/j.egypro.2011.01.028.

[31] Y. Wang, M. Fang, T. Wang, J. Gao, Y. Huang, S. Li, X. Lu, Y. Sun, F. Zhang, Corrosion performance of carbon/stainless steel in amine-based solvents under different conditions for CO_2 chemical absorption process, Greenh. Gases Sci. Technol. 14 (2024) 26–41, https://doi.org/10.1002/ghg.2250.

[32] Y. Xiang, Y.S. Choi, Y. Yang, S. Nešić, Corrosion of carbon steel in MDEA-based CO_2 capture plants under regenerator conditions: effects of O_2 and heat-stable salts, Corrosion 71 (2015) 30–37, https://doi.org/10.5006/1354.

[33] Y. Xiang, M. Yan, Y.S. Choi, D. Young, S. Nesic, Time-dependent electrochemical behavior of carbon steel in MEA-based CO_2 capture process, Int. J. Greenh. Gas Control 30 (2014) 125–132, https://doi.org/10.1016/j.ijggc.2014.09.003.

[34] N. Kladkaew, R. Idem, P. Tontiwachwuthikul, C. Saiwan, Corrosion behavior of carbon steel in the monoethanolamine-H_2O-CO_2-O_2-SO_2 system: products, reaction pathways, and kinetics, Ind. Eng. Chem. Res. 48 (2009) 10169–10179, https://doi.org/10.1021/ie900746g.

[35] Z. Yin, W. Zhao, Z. Bai, Y. Feng, Characteristics of CO_2 corrosion scale formed on P110 steel in simulant solution with saturated CO_2, Surf. Interf. Anal. 40 (2008) 1231–1236, https://doi.org/10.1002/sia.2867.

[36] A. Veawab, P. Tontiwachwuthikul, S.D. Bhole, Studies of corrosion and corrosion control in a CO_2 −2-amino-2-methyl-1-propanol (AMP) environment, Ind. Eng. Chem. Res. 36 (1997) 264–269, https://doi.org/10.1021/ie9504563.

[37] I.J. Uyanga, R.O. Idem, Studies of SO_2- and O_2-induced degradation of aqueous MEA during CO_2 capture from power plant flue gas streams, Ind. Eng. Chem. Res. 46 (2007) 2558–2566, https://doi.org/10.1021/ie0614024.

[38] A. Bello, R.O. Idem, Comprehensive study of the kinetics of the oxidative degradation of CO_2 loaded and concentrated aqueous monoethanolamine (MEA) with and without sodium metavanadate during CO_2 absorption from flue gases, Ind. Eng. Chem. Res. 45 (2006) 2569–2579, https://doi.org/10.1021/ie050562x.

[39] B. Udayappan, A. Veawab, Performance analysis of methionine as an environmentally friendly corrosion inhibitor for carbon steel in the amine based carbon capture process, Int. J. Greenh. Gas Control 114 (2022) 103565, https://doi.org/10.1016/j.ijggc.2021.103565.

[40] A.G. Talkhan, A. Benamor, M.S. Nasser, H. Qiblawey, S.A. El-Tayeb, S.M. El-Marsafy, Corrosion study of carbon steel in CO_2 loaded solution of N-methyldiethanolamine and L-arginine mixtures, J. Electroanal. Chem. 837 (2019) 10–21, https://doi.org/10.1016/j.jelechem.2019.02.008.

[41] A. Sedik, S. Athmani, A. Saoudi, H. Ferkous, N. Ribouh, D. Lerari, K. Bachari, S. Djellali, M. Berredjem, R. Solmaz, M. Alam, B.H. Jeon, Y. Benguerba, Experimental and theoretical insights into copper corrosion inhibition by protonated amino-acids, RSC Adv. 12 (2022) 23718–23735, https://doi.org/10.1039/d2ra03535a.

[42] P.C. Okafor, Y. Zheng, Synergistic inhibition behaviour of methylbenzyl quaternary imidazoline derivative and iodide ions on mild steel in H_2SO_4 solutions, Corros. Sci. 51 (2009) 850–859, https://doi.org/10.1016/j.corsci.2009.01.027.

[43] J.Z. Ai, X.P. Guo, J.E. Qu, Z.Y. Chen, J.S. Zheng, Adsorption behavior and synergistic mechanism of a cationic inhibitor and KI on the galvanic electrode, Colloids Surf. A Physicochem. Eng. Asp. 281 (2006) 147–155, https://doi.org/10.1016/j.colsurfa.2006.02.031.

[44] G. Fytianos, S.J. Vevelstad, H.K. Knuutila, Degradation and corrosion inhibitors for MEA-based CO_2 capture plants, Int. J. Greenh. Gas Control 50 (2016) 240–247, https://doi.org/10.1016/j.ijggc.2016.05.003.

[45] Y. Zhu, Q. Sun, Y. Wang, J. Tang, Y. Wang, H. Wang, Molecular dynamic simulation and experimental investigation on the synergistic mechanism and synergistic effect of oleic acid imidazoline and L-cysteine corrosion inhibitors, Corros. Sci. 185 (2021) 109414, https://doi.org/10.1016/j.corsci.2021.109414.

[46] H. Lgaz, D.E. Lee, A. Aldalbahi, H. Seung Lee, How does the integration of amino acids enhance the bonding ability of triazine-based inhibitors with iron surfaces: Insights from SCC-DFTB, COSMO-RS and molecular dynamics simulations, J. Mol. Liq. 414 (2024), https://doi.org/10.1016/j.molliq.2024.126274.

[47] L. Kollias, D. Zhang, S.I. Allec, M.T. Nguyen, M.S. Lee, D.C. Cantu, R. Rousseau, V. A. Glezakou, Advanced theory and simulation to guide the development of CO_2 capture solvents, ACS Omega 7 (2022) 12453–12466, https://doi.org/10.1021/acsomega.1c07398.

[48] B. El Ibrahimi, A. Jmiai, L. Bazzi, S. El Issami, Amino acids and their derivatives as corrosion inhibitors for metals and alloys, Arab. J. Chem. 13 (2020) 740–771, https://doi.org/10.1016/j.arabjc.2017.07.013.

[49] B. El Ibrahimi, A.A. Addi, L. Guo, S. Kaya, Molybdates as corrosion inhibitors, Inorg. Anticorros. Mater. Past, Present Futur. Perspect. (2021) 297–321, https://doi.org/10.1016/B978-0-323-90410-0.00016-7.

[50] M.A. Ahmed, S. Amin, A.A. Mohamed, Current and emerging trends of inorganic, organic and eco-friendly corrosion inhibitors, RSC Adv. 14 (2024) 31877–31920, https://doi.org/10.1039/d4ra05662k.

[51] A.Y. Musa, R.T.T. Jalgham, A.B. Mohamad, Molecular dynamic and quantum chemical calculations for phthalazine derivatives as corrosion inhibitors of mild steel in 1M HCl, Corros. Sci. 56 (2012) 176–183, https://doi.org/10.1016/j.corsci.2011.12.005.

[52] M.E. Belghiti, S. Echihi, A. Mahsoune, Y. Karzazi, A. Aboulmouhajir, A. Dafali, I. Bahadur, Piperine derivatives as green corrosion inhibitors on iron surface; DFT, Monte Carlo dynamics study and complexation modes, J. Mol. Liq. 261 (2018) 62–75, https://doi.org/10.1016/j.molliq.2018.03.127.

[53] S.J. Vevelstad, I. Eide-Haugmo, E.F. Da Silva, H.F. Svendsen, Degradation of MEA A theoretical study, Energy Procedia 4 (2011) 1608–1615, https://doi.org/10.1016/j.egypro.2011.02.031.

[54] G.S. Goff, G.T. Rochelle, Monoethanolamine degradation: O_2 mass transfer effects under CO_2 capture conditions, Ind. Eng. Chem. Res. 43 (2004) 6400–6408, https://doi.org/10.1021/ie0400245.

[55] P.C. Rooney, M.S. DuPart, T.R. Bacon, Oxygen's role in alkanolamine degradation, Hydrocarb. Process. 77 (1998) 109–113.

[56] S. Sjostrom, K.E. Baldrey, C. Senior, Control of wet scrubber oxidation inhibitor and byproduct recovery, (2018). https://patentimages.storage.googleapis.com/11/a5/79/883be2e7659114/US10159931.pdf.

[57] Y.J. Lee, G.T. Rochelle, Oxidative degradation of organic acid conjugated with sulfite oxidation in flue gas desulfurization: products, kinetics, and mechanism, Environ. Sci. Technol. 21 (1987) 266–272, https://doi.org/10.1021/es00157a007.

[58] Y. Marcus, On water structure in concentrated salt solutions, J. Solution Chem. 38 (2009) 513–516, https://doi.org/10.1007/s10953-009-9398-z.

[59] T. Supap, C. Saiwan, R. Idem, P.P.T. Tontiwachwuthikul, Part 2: Solvent management: solvent stability and amine degradation in CO_2 capture processes, Carbon Manag. 2 (2011) 551–566, https://doi.org/10.4155/cmt.11.55.

[60] F. Zhao, C. Cui, S. Dong, X. Xu, H. Liu, An overview on the corrosion mechanisms and inhibition techniques for amine-based post-combustion carbon capture process, Sep. Purif. Technol. 304 (2023) 122091, https://doi.org/10.1016/j.seppur.2022.122091.

[61] G. Li, K. Sheng, Y. Lei, J. Yang, Y. Chen, X. Guo, G. Chen, B. Chang, T. Wu, X. Wang, Facile synthesis of Fe3C-dominated Fe/Fe_3C/$FeN_{0.0324}$ multiphase nanocrystals embedded in nitrogen-modified graphitized carbon as efficient pH-universal catalyst for oxygen reduction reaction and zinc-air battery, Chem. Eng. J. 451 (2023) 138823, https://doi.org/10.1016/j.cej.2022.138823.

[62] H. Lepaumier, E.F. Da Silva, A. Einbu, A. Grimstvedt, J.N. Knudsen, K. Zahlsen, H. F. Svendsen, Comparison of MEA degradation in pilot-scale with lab-scale experiments, Energy Procedia 4 (2011) 1652–1659, https://doi.org/10.1016/j.egypro.2011.02.037.

[63] J. Jackson, M. Finšgar, Application of corrosion inhibitors for steels in acidic media for the oil and gas industry : a review, Corros. Sci. 86 (2014) 17–41.

[64] B. Lin, J. Tang, Y. Wang, H. Wang, Y. Zuo, Study on synergistic corrosion inhibition effect between calcium lignosulfonate (CLS) and inorganic inhibitors on Q235 carbon steel in alkaline environment with Cl−, Molecules 25 (2020) https://doi.org/10.3390/molecules25184200.

[65] D. Özkir, K. Kayakirilmaz, E. Bayol, A.A. Gürten, F. Kandemirli, The inhibition effect of Azure a on mild steel in 1M HCl. a complete study: adsorption, temperature, duration and quantum chemical aspects, Corros. Sci. 56 (2012) 143–152, https://doi.org/10.1016/j.corsci.2011.11.010.

[66] M. Şahin, G. Gece, F. Karcı, S. Bilgiç, Experimental and theoretical study of the effect of some heterocyclic compounds on the corrosion of low carbon steel in 3.5% NaCl medium, J. Appl. Electrochem. 38 (2008) 809–815, https://doi.org/10.1007/s10800-008-9517-3.

[67] P. Rg, Y. W, Density functional approach to the frontier-electron theory of chemical reactivity, J. Am. Chem. Soc. 106 (1984) 4049–4050.